ISSN 1061-933X, Colloid Journal, 2011, Vol. 73, No. 6, pp. 761–767. © Pleiades Publishing, Ltd., 2011.
Original Russian Text © A.E. Galashev, V.A. Polukhin, 2011, published in Kolloidnyi Zhurnal, 2011, Vol. 73, No. 6, pp. 764–771.

Computer-Assisted Study of Silver Absorption by Porous Silicon Dioxide Nanoparticles

A. E. Galashev[a] and V. A. Polukhin[b]

[a] *Institute of Industrial Ecology, Ural Division, Russian Academy of Sciences, ul. Sof'i Kovalevskoi 20, Yekaterinburg, 620990 Russia*

[b] *Institute of Metallurgy, Ural Division, Russian Academy of Sciences, ul. Amundsena 101, Yekaterinburg, 620990 Russia*

Received December 20, 2010

Abstract—The absorption of silver atoms by porous silicon dioxide particles is studied by the molecular dynamics method. Upon the absorption of silver atoms, $(SiO_2)_{50}$ nanoparticles do not increase their volume. A particle is divided into two unequal parts by an island shell formed from SiO_2 structural units, which causes anisotropy in the electrical and thermal conductivity of the nanocomposite. IR absorption and emission spectra, Raman spectra, as well as the number of electrons active with respect to IR radiation are calculated. The calculated absorption spectra show the mode corresponding to the stretching vibrations of Si–O surface groups. The addition of silver atoms to nanoparticles can enhance significantly the power of heat radiation emission.

DOI: 10.1134/S1061933X11050036

INTRODUCTION

Optical (or laser) forceps are a device in which a focused laser beam is used to displace microscopic objects or to retain these objects at a certain site. Light acts on surrounding objects rather weakly, but its action appears to be sufficient to draw nanoparticles into the laser beam focus. When a particle occurs in the focus, it can be displaced by the laser beam. To use the forces created by the optical forceps light, the particle must be polarized in an external electric field with the formation of bound surface charges. In this case, the bound charges must generate a field opposite to the external one in order to draw the particle into the focus zone. If the permittivity of a dispersion medium exceeds the permittivity of the material of the particle, the latter will be forced out of the focus zone. Analogously, if the absolute refractive index of the particle material is lower than that of the dispersion medium, it will be moved away from the beam axis, as can be easily seen from the character of light beam refraction. Thus, the optical forceps works better if the particle material has a high relative refractive index.

Recently, a great deal of attention has been devoted to the development and refinement of optical forceps [1–6]; however, the properties of dielectric–metal [7] and dielectric–semiconductor [8] hybrid nanoparticles have been much less studied. Upon electromagnetic radiation scattering, metal-coated dielectric particles are characterized by a high signal-to-noise ratio and can be used as biosensors [9, 10]. The theoretical description of the behavior of uncharged particles used in single-beam gradient optical forceps depends on the ratio of the particle size to the radiation wavelength. Particles with sizes much smaller than the wavelength can be considered as induced dipoles oscillating in an electric field [11]. The force acting on a particle in a beam is presented by two components; one of them is related to light scattering and acts in a direction of incident light, and another one is due to the gradient of radiation intensity and is determined by the gradient value. The particle is completely captured by the beam, when the gradient force exceeds the force of the light scattering. In this case, the particle falls in a rather deep potential well, which it cannot leave as a result of Brownian motion. The force generated by light scattering is mainly determined by the particle size, and the gradient force is governed by its polarizability [12–14].

As is known from experimental data, due to the high polarizability of metal particles, their gradient force significantly exceeds that for dielectric particles [15, 16]. However, metal particles of micron sizes can hardly be captured by a laser beam because of their significant light scattering. Hybrid particles (with a dielectric core and a metal shell) are optimal for control by beams because they have a high polarizability at a low scattering cross section. These hybrid nanoparticles were obtained by depositing gold or silver layers of different thicknesses on silicon dioxide particles [16].

Electron properties of small clusters $Ag(SiO_2)_n$ ($n = 1–7$) were studied by the density functional theory [17]. These clusters can be the alternative to the more expensive $(Au)_i(SiO_2)_n$ system, since their prop-

Parameters of potentials

q_O, e	q_{Si}, e	q_{Ag}, e	$\alpha^{(p)}_{SiO_2}$, Å^3	σ^{LJ}_{Ag-Si}, nm
−1.38257	2.76514	0	3.219	0.339
γ_{O-O}	γ_{Si-O}	γ_{Si-Si}	γ_{Ag-Ag}	σ^{LJ}_{Ag-O}, nm
12.07092	11.15230	10.45517	8.52887	0.285
D_{O-O}, kJ/mol	D_{Si-O}, kJ/mol	D_{Si-Si}, kJ/mol	D_{Ag-Ag}, kJ/mol	ε^{LJ}_{Ag-Si}, kJ/mol
0.32830	2.52487	2.76538	32.06025	20.55611
r^0_{O-O}, nm	r^0_{Si-O}, nm	r^0_{Si-Si}, nm	r^0_{Ag-Ag}, nm	ε^{LJ}_{Ag-O}, kJ/mol
0.37942	0.24538	0.30429	0.31150	4.56498

erties are rather similar. The practical use of clusters containing several metal atoms encounters significant difficulties. For many applications, the needed average size of clusters must not exceed several nanometers. The capability of small (2–3 nm) porous SiO_2 particles to absorb Ag atoms has not yet been studied.

The goal of this work was to study the absorption of silver atoms by a porous nanoparticle $(SiO_2)_{50}$ with a transverse size of ≈2.24 nm, to calculate the frequency dependence of IR absorption coefficient, and to determine the Raman spectra and the electron densities before and after the addition of silver atoms to $(SiO_2)_{50}$ particles.

MOLECULAR DYNAMICS MODEL

In this work, the pair interactions in the SiO_2 system were described using the Coulomb and Morse potentials [18] as follows:

$$\Phi(r_{ij}) = \frac{q_i q_j}{r_{ij}} + D_{ij}\left[\exp\left\{\gamma_{ij}\left[1 - r_{ij}/r_{ij}^0\right]\right\} - 2\exp\left\{\frac{\gamma_{ij}}{2}\left[1 - r_{ij}/r_{ij}^0\right]\right\}\right], \quad (1)$$

where the interaction between i- and j-type atoms is determined by parameters q_i, q_j, D_{ij}, γ_{ij}, r_{ij}^0 (see table), and the distance between these atoms r_{ij}. The cutoff radius of this potential was 0.9 nm. In addition to the pair potential, the effects of dipole polarization were taken into account. The polarizability $\alpha^{(p)} = 3.219$ Å, which corresponds to the experimental polarizability of a SiO_2 molecule, was related to the center of masses of this structural unit. The Si–O distance in the structural unit was equal to the minimum distance r_{Si-O} = 0.162 nm in a quartz crystal, while the O–Si–O angle was equal to a tetrahedral angle of 109.5°.

The interactions between silver atoms in the model were described via the Morse potential [19]; its parameters are given in the table. The Si–Ag and O–Ag atom–atom interactions were specified by the Lennard-Jones potential with parameters σ^{LJ} and ε^{LJ} taken from [20]. These parameters are also listed in the table.

Flexible molecular models were used in the calculations. The molecules were provided with flexibility via the procedure developed according to the Hamilton dynamics [21, 22]. Let us consider a diatomic molecule. Assume that atoms a and b in the molecule are located at a distance

$$q = |\mathbf{r}_a - \mathbf{r}_b|,$$

where $\mathbf{r}_a$ and $\mathbf{r}_b$ are vectors, which determine the positions of the atoms. If the atomic masses are denoted as m_a and m_b, the reduced mass is defined by the following expression:

$$\mu = \frac{m_a m_b}{m_a + m_b}. \quad (2)$$

Atoms a and b are retained in the molecule because the total potential force $\mathbf{f}(\mathbf{q}) = -\frac{\partial \mathbf{r}}{\partial \mathbf{q}}\nabla\Phi(\mathbf{r})$ is equilibrated by the centrifugal force $-\mu q\omega^2$; hence,

$$-\mu q\omega^2 - \mathbf{f}(\mathbf{r})\frac{\partial \mathbf{r}}{\partial \mathbf{q}} = 0,$$

where $\omega = |\mathbf{v}_a - \mathbf{v}_b|/q$ is angular velocity, while $\mathbf{v}_a$ and $\mathbf{v}_b$ are the velocities of a and b atoms. For a polyatomic molecule, the contribution to potential energy U is minimized with respect to each generalized coordinate as follows [23]:

$$\frac{\partial}{\partial q_i} H(\mathbf{r}, \mathbf{v}) = \frac{\partial}{\partial q_i}\left(\frac{1}{2}\mu_i q_i^2 \omega_i^2 + U(\mathbf{r})\right) = 0.$$

The initial configuration of a $(SiO_2)_{50}$ nanoparticle was created in two stages. At the first stage, a fragment of β quartz was obtained in the form of a rectangular

parallelepiped containing 32 Si atoms and 64 O atoms using a GRINSP program [24] based on the Monte Carlo method. The second stage involved the assembly of 27 identical fragments of β quartz into a larger rectangular parallelepiped consisting of a central parallelepiped and 26 similar parallelepipeds surrounding it. All parallelepipeds had identical orientation determined by the arrangement of the atoms. The minimum distances between atoms (of both the same and different types) that belong to different parallelepipeds were no less than the corresponding distances between atoms that belong to the same parallelepiped, but did not exceed the latter by more than $0.1a$ ($a = 0.4997$ nm, $c = 0.5460$ nm, $\alpha = \beta = 90°$, and $\gamma = 120°$ are the parameters of the β quartz cell). β-Quartz represents a hexagonal crystallographic system. Then, a sphere containing 50 Si atoms was drawn from the center of masses of the assembled parallelepiped and, for each of these atoms, the pair of the nearest O atoms was found. Thus, SiO_2 structural units were formed in the obtained package. As the volume of the resulting $(SiO_2)_{50}$ nanoparticle was larger than the volume of the central parallelepiped, cavities were formed at the junctions of parallelepipeds in this nanoparticle. The density of the nanoparticle thus obtained was equal to 1.55 g/cm^3. Remember that the density of β quartz is 2.53 g/cm^3.

The initial velocities of SiO_2 particles were chosen randomly; they were fitted to 293 K by distributing supplied or removed heat energy over molecules in proportion to the absolute values of their velocities. Then, a preliminary molecular-dynamic calculation was carried out for the formed nanoparticle $(SiO_2)_{50}$. The calculation time included 10^6 time steps with step duration $\Delta t = 10^{-16}$ s. During this period of time, the system under investigation was equilibrated that was confirmed by the establishment of the Maxwell distribution for the velocities of SiO_2 objects. In this case, the nanoparticle structure relaxed to the energetically favorable packing ($U \approx -0.9$ eV/particle). Then, at a certain time moment taken as zero ($t = 0$), silver atoms were incorporated into the environment of the $(SiO_2)_{50}$ nanoparticle. The positions of Ag atoms were determined with the help of a virtual fcc lattice penetrating the $(SiO_2)_{50}$ cluster. Lattice parameter a was equal to 0.6 nm. Note that silver has fcc lattices with parameter $a = 4.0772$ Å (at 293 K). The lattice sites nearest to the silicon dioxide nanoparticle, which were located at a distance of no less than 0.6 nm from each Si or O atom, were determined and silver atoms were placed into them. Three calculations were carried out at different numbers of silver atoms N_{Ag} surrounding the $(SiO_2)_{50}$ nanoparticle: $N_{Ag} = 10$, 30, and 50. In each case, the basic calculation was preceded by a preliminary calculation period of $0.1 \times 10^6 \Delta t$, during which the necessary structural relaxation of the system took place. The basic calculation of the spectral characteristics lasted $2.5 \times 10^6 \Delta t$ for the $(SiO_2)_{50}$, $Ag_{10}(SiO_2)_{50}$, $Ag_{30}(SiO_2)_{50}$, and $Ag_{50}(SiO_2)_{50}$ systems (I, II, III, and IV, respectively), which were composed of the $(SiO_2)_{50}$ cluster surrounded by Ag atoms (for systems II–IV).

The nearest environment of atoms in the nanoparticles was analyzed on the basis of polyhedron construction. When considering the environment formed from Si atoms around a Si center, the Voronoi polyhedrons (VPs) were constructed and, when studying the environment formed from O atoms around the same center, combined polyhedrons (CPs) were constructed. Using the polyhedrons of both types, the number of geometric neighbors (Si or O) was found, and the rings formed from atoms of the same type, the average number of units in these rings, the number of Si–Si and Si–O bonds per one atom, and the lengths of these bonds were determined. Given this, a geometric criterion was introduced for Si–Si and Si–O bonds with threshold values of 3.5 and 2.5 Å, respectively.

The molecular dynamics calculations were implemented using the program written in the PASCAL algorithmic language. The equations that describe the motion of the centers of masses of SiO_2 structural units and Ag atoms were integrated by the fourth-order Gear method [25]. The equations for the rotary motion of the structural units were analytically solved using the Rodrigue–Hamilton parameters [26], while the scheme of integration of motion equations in the presence of rotations corresponded to the approach proposed by Sonnenschein [27]. The calculations were carried out on a Pentium-IV four-core computer operating at the clock frequency of the processor equal to 2.83 GHz.

DIELECTRIC PROPERTIES

The method used to calculate complex permittivity $\varepsilon(\omega) = \varepsilon'(\omega) - i\varepsilon''(\omega)$ is described in [28, 29]. Absorption coefficient α of external IR radiation can be presented via function $\varepsilon''(\omega)$ in the following form [20]:

$$\alpha(\omega) = 2\frac{\omega}{c}\mathrm{Im}[\varepsilon(\omega)^{1/2}].$$

For depolarized light, the Raman spectrum $J(\omega)$ is expressed by the following equation [30]:

$$J(\omega) = \frac{\omega}{(\omega_L - \omega)^4}\left(1 - e^{-\hbar\omega/kT}\right) \times \mathrm{Re}\int_0^\infty dt e^{i\omega t}\langle \Pi_{xz}(t)\Pi_{xz}(0)\rangle,$$

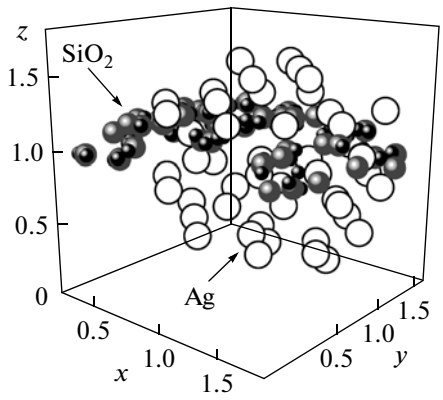

Fig. 1. Configuration of $Ag_{50}(SiO_2)_{50}$ nanoparticle at 250-ps time moment. Coordinates of atoms are given in nm.

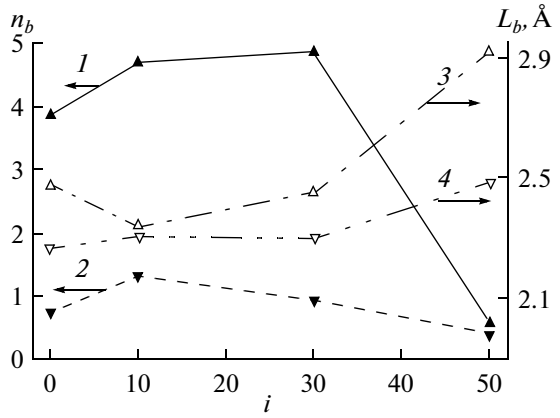

Fig. 2. Numbers of (*1*) Si–Si and (*2*) Si–O bonds per atom and average lengths of (*3*) Si–Si and (*4*) Si–O bonds in $Ag_i(SiO_2)_{50}$ nanoparticles.

where

$$\Pi(t) \equiv \sum_{j=1}^{N}\left[\boldsymbol{\alpha}_j^{(p)}(t) - \left\langle \boldsymbol{\alpha}_j^{(p)} \right\rangle\right],$$

ω_L is the frequency of an exciting laser, Π_{xz} is the xz component of $\Pi(t)$, $\hbar$ is the Planck constant, T is temperature, k is the Boltzmann constant, the x axis is directed along a molecular dipole, and xOy is the molecular plane. ω_L = 19 436.3 cm^{-1}(green line of argon laser, λ = 514.5 nm) was used in the simulation.

The frequency dispersion of permittivity determines the frequency dependence of dielectric loss $P(\omega)$ through the following expression [31]:

$$P = \frac{\varepsilon''\langle E^2\rangle\omega}{4\pi},$$

where $\langle E^2\rangle$ is the mean square of electric field intensity and ω is the frequency of emitted electromagnetic wave.

The total number N_{el} of electrons, which interact with the external electromagnetic field, per unit volume of the cluster is given as [32]

$$N_{el} = \frac{m}{2\pi^2 e^2}\int_0^\infty \omega\varepsilon''(\omega)\,d\omega,$$

where e and m are the electron charge and mass.

CALCULATION RESULTS

The absorption of Ag atoms is not accompanied by any increase in the $(SiO_2)_{50}$ nanoparticle size. Furthermore, after the absorption of 10, 30, and 50 Ag atoms, the maximum size (the distance between two outermost atoms) of the nanoparticle slightly shortens by 0.022, 0.023, and 0.11%, respectively. This is explained by the fact that the free volume in the porous $(SiO_2)_{50}$ nanoparticle is 3.3-fold larger than the volume of a solid Ag_{50} cluster. Ag atoms tend to densification, i.e., the formation of solid silver corresponding to the thermodynamic parameters of the model. The motion of Ag atoms located in pores of SiO_2 skeleton cannot lead to an essential change in the SiO_2 structure, since the Si–O bond energy is 3.8 times higher than the bond energy of Ag_2 dimer. The formation of a shell (crust) from SiO_2 is mainly determined by the type of Si–O interactions and occurs during initial 10 ps, i.e., during the first 10^5 time steps. During the further slow relaxation of the structure, the nanoparticle size increases by 0.02 and 0.003% after the absorption of 10 and 30 Ag atoms, respectively, and decreases by 0.0008% after the absorption of 50 Ag atoms. Figure 1 shows the $Ag_{50}(SiO_2)_{50}$ cluster configuration obtained by the 250-ps time moment. It is evident that the interaction with Ag atoms does not hinder the formation of the crust from SiO_2. The crust has the form of connected islands. In turn, the presence of SiO_2 crust does not prevent the silver cluster from retaining its spherical shape. Ag atoms are in close contact with Si and O atoms and fill the gaps between the SiO_2 structural units. The internal zone of the silver cluster, which is in contact with the crust, is disordered. However, at the periphery, a crystalline order is observed, which is inherited from the initial fcc packing of Ag atoms. The observed structural relaxation is mainly related to the movement of lighter and more mobile SiO_2 structural units.

Figure 2 demonstrates a change in the number of Si–Si and Si–O bonds n_b per an atom upon the addition of Ag atoms to the cluster. The number of Si–Si bonds slightly increases (by 2.6%) as a result of adding up to 30 Ag atoms to the cluster. However, when 50 Ag atoms were added to the cluster, n_b^{Si-Si} decreased considerably (by 88% compared to n_b^{Si-Si} at i = 30). The number of Si–O bonds increased (by 42.8%) after the capture of 10 Ag atoms and decreased by 46.0% after

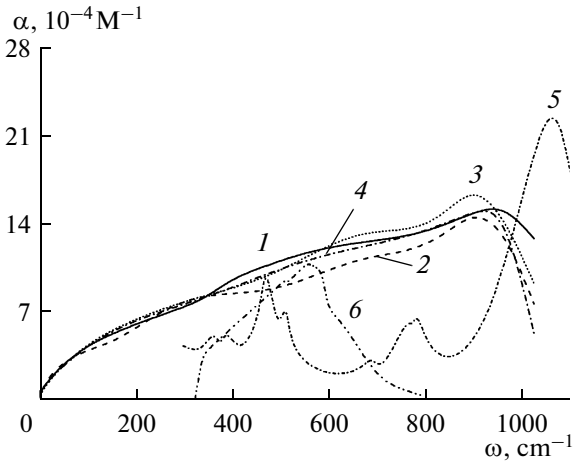

Fig. 3. Coefficients of IR radiation absorption by systems formed from $(SiO_2)_{50}$ cluster and Ag atoms: (*1–4*) systems I–IV, (*5*, *6*) experimental α(ω) spectra for α quartz [34] and silver nanoparticles in SiO_2 matrix with pore sizes of 100–1000 nm [35], respectively, at 300 K.

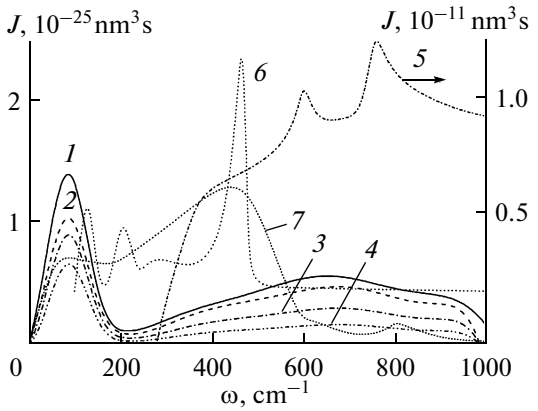

Fig. 4. Raman spectra of systems formed from $(SiO_2)_{50}$ cluster and Ag atoms: (*1–4*) systems I–IV, (*5*) spectrum of surface-enhanced Raman scattering for silver nanoparticle coated with SiO_2 [16], (*6*, *7*) experimental Raman spectra of α quartz [36] and fused quartz [37], respectively, at 300 K.

the addition of 50 Ag atoms to the cluster. The length of Si–Si bonds, L_b^{Si-Si}, initially diminishes (as a result of the addition of 10 Ag atoms), and then grows with the number of silver atoms in the system. At $i = 50$, the gain in the bond length L_b^{Si-Si} was as high as 17.2%. Even upon the addition of 10 Ag atoms to the cluster, the length of Si–O bonds increased by 1.6%, while the final gain in the L_b^{Si-Si} value at $i = 50$ was 9.2%. Ag atoms were not included into the neighbors upon the construction of both VPs and CPs. However, their presence leads to significant structural changes that result in the significant depletion of the polyhedron distribution with respect to the number of faces and the distribution of faces over the number of sides (angles). At $i = 50$, the distribution of VPs is presented only by tridecahedrons and 60% CPs are heptadecahedrons.

The frequency spectrum of the IR absorption α(ω) shows that, in the frequency range of $0 \le \omega \le 1000$ cm^{-1}, the effect of absorption of Ag atoms on the absorbance of the silicon dioxide cluster is insignificant (Fig. 3). The integral intensities of α(ω) spectra for systems I–IV are related as 1 : 0.89 : 0.99 : 0.94 and the intensity ratio of their main peaks is 1 : 0.96 : 1.10 : 0.99. Pure silver does not contribute to the IR absorption spectrum. The peaks of the $\alpha(\omega)$ spectra for systems I–IV are observed in the frequency range of 907–945 cm^{-1}. This range is attributed to the stretching vibrations of the surface Si–O groups. The peak at 940 cm^{-1} in a dry silicon dioxide gel is due to the vibrations of Si–O groups as the components of stretching vibrations of Si–OH [33]. This peak indicates the presence of silanol Si–OH groups in the dry gel; the intensity of this peak decreases in the course of gel densification. The changes in this peak intensity lead us to conclude that, depending on the number of absorbed Ag atoms, either the densification (at $N_{Ag} = 10$ and 50) or the loosening (at $N_{Ag} = 30$) of the model SiO_2 structure can take place. The drop in the integral intensity of $\alpha(\omega)$ spectra is accompanied by the elongation of both Si–Si and of Si–O bonds. The minimum intensity of the main peak is observed at the maximum number of Si–O bonds in the system. After the absorption of Ag atoms, the position of the most intense peak in the $\alpha(\omega)$ spectra of the clusters is shifted to the low-frequency region by 32, 41, and 22 cm^{-1} for systems II, III, and IV, respectively. The experimental IR absorption spectrum of α quartz displays the most pronounced peak at 1065 cm^{-1} [34], and the maximum in the α(ω) spectrum of system I is observed at 942 cm^{-1}. The $\alpha(\omega)$ spectrum of the Ag–SiO_2 nanocomposite with pore sizes of 100–1000 nm shows the maximum at a still lower frequency (565 cm^{-1}) [35] than the $\alpha(\omega)$ spectra of systems I–IV.

The integral intensity of the Raman spectrum $J(\omega)$ gradually decreases as new Ag atoms are added to the $(SiO_2)_{50}$ cluster (Fig. 4), with the ratio between the integral intensities for systems I–IV being equal to 1 : 0.81 : 0.56 : 0.34. In this case, the position of the first peak (at 87 cm^{-1}) remains unchanged, and the diffuse second peak is shifted to higher frequencies. The experimental Raman spectrum of α quartz is characterized by four peaks in the frequency range of $100 \le \omega \le 500$ cm^{-1}, with the main peak being observed at 470 cm^{-1} [36]. In addition, Fig. 4 shows the anti-Stokes scattered intensity for fused quartz at 300 K [37]. The position of the first maximum in this spectrum is in a good accordance with the location of the first peaks in the $J(\omega)$ spectra of the cluster sys-

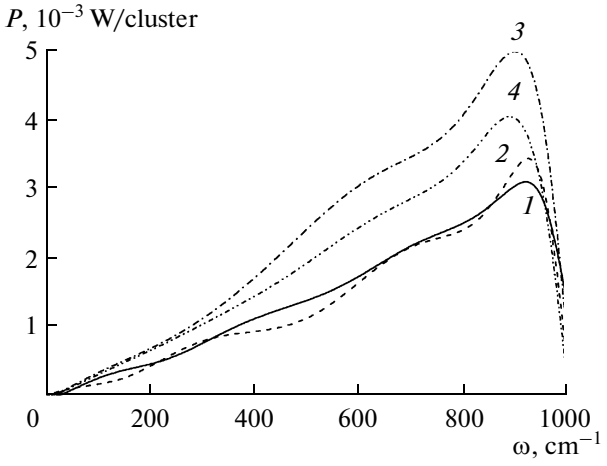

Fig. 5. IR emission spectra for $Ag_i(SiO_2)_{50}$ clusters, $i = 0$–50; curves *1*–*4* correspond to systems I–IV.

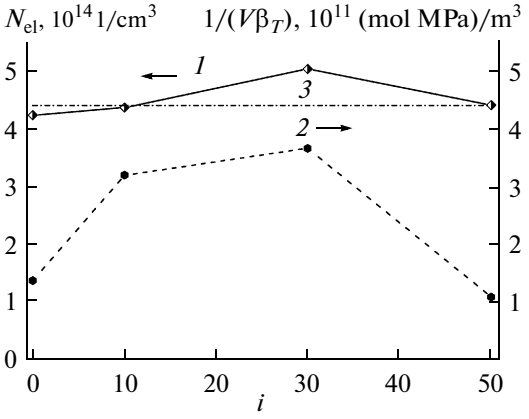

Fig. 6. (*1*) Number of electrons interacting with external electromagnetic radiation and (*2*) mechanical stability coefficient versus number of silver atoms in $Ag_i(SiO_2)_{50}$ clusters; (*3*) mechanical stability coefficient of α quartz.

tems, while the second maximum is in the vicinity of the most intense peak in the $J(\omega)$ spectrum of α quartz. The surface-enhanced Raman spectrum of a silver nanoparticle coated with SiO_2 [16] has the shape corresponding to the $J(\omega)$ spectrum in the region of the second diffuse peak for systems I–IV except for the features observed at 603 and 762 cm^{-1}. Upon the addition of Ag atoms, which have much higher volume polarizability α^p (7.9 Å^3) than that of silicon dioxide (3.219 Å^3), to a $(SiO_2)_{50}$ nanoparticle, the average polarizability of the structural unit $\bar{\alpha}^p$ increases compared to the value calculated for the $(SiO_2)_{50}$ cluster. The effect of Ag atoms on the dielectric characteristics of the nanoparticle becomes stronger with their number; however, the disordering of dipole moments simultaneously increases. Therefore, the fluctuations of α^p gradually decrease. As a result, the intensity of the $J(\omega)$ spectra for silver-containing systems decreases with a rise in the number of Ag atoms. Due to the stochastic behavior of the total dipole moment, the intensity of reproducible peak and the total intensity of the IR spectrum change insignificantly and randomly with increasing number of Ag atoms in the cluster.

The addition of 10 Ag atoms to the silicon dioxide cluster does not increase the power of the emitted IR radiation (Fig. 5). However, after the addition of 30 Ag atoms to the $(SiO_2)_{50}$ cluster, the total power of the emitted heat radiation P_{tot} considerably rises. The absorption of 50 Ag atoms leads to some reduction in the emission power compared to P_{tot} of the $P(\omega)$ spectrum for system III, but this characteristic increases compared to system I. The following ratio between P_{tot} values of systems I–IV is observed: 1 : 0.96 : 1.56 : 1.28. Thus, for the maximal enhancement of the power of IR radiation emission, some optimum number of Ag atoms must be added to the $(SiO_2)_{50}$ cluster.

The dependence of the number of electrons N_{el} participating in the interaction with IR radiation on the number i of Ag atoms in the cluster has a maximum at $i = 30$ (Fig. 6, curve *1*). For the cluster with 30 Ag atoms, N_{el} is 1.6-fold larger than that for the $(SiO_2)_{50}$ cluster. Moreover, silicon dioxide cluster with 30 Ag atoms turns out to be most stable according to the mechanical criterion of stability $(1/V\beta_T > 0)$, where V and β_T are the volume and isothermal compressibility of the cluster, respectively. The method for calculating β_T is described in [38]. For the studied clusters, isodynamic stability coefficient $1/V\beta_T$ has a maximum value at $i = 30$ (Fig. 6, curve *2*). For the clusters, coefficients $1/V\beta_T$ are lower than those for α quartz (Fig. 6, curve *3*).

CONCLUSIONS

The absorption of Ag atoms in a high-porosity $(SiO_2)_{50}$ nanoparticle formed from SiO_2 structural units is accompanied by a structural transition. In the presence of Ag atoms, a loose spherical $(SiO_2)_{50}$ nanoparticle changes its shape and is transformed into an island shell. The part of the system that represents an Ag lattice becomes denser and captures the SiO_2 shell. In this situation, the volume of a $(SiO_2)_{50}$ nanoparticle does not increase after the absorption Ag atoms. The addition of silver atoms to the $(SiO_2)_{50}$ nanoparticle does not enhance the IR absorption coefficient; however, it decreases the intensity of Raman spectra and noticeably enhances the power of heat radiation emitted by the clusters. Moreover, the number of electrons active with respect to IR radiation enlarges and, at a moderate number of absorbed Ag atoms, the mechanical stability of the cluster rises. Due to the high ther-

mal conductivity of silver, the effective transfer of emitted energy to objects contacting with the clusters may be expected. The structure of the formed nanocomposite suggests the anisotropic character of its electrical and thermal conductivity.

REFERENCES

1. Molloy, J.E. and Padgett, M.J., *Contemp. Phys.*, 2002, vol. 43, p. 241.
2. Molloy, J.E., Dholakia, K., and Padgett, M.J., *J. Mod. Opt.,* 2003, vol. 50, p. 1501.
3. Grier, D.G., *Nature* (London), 2003, vol. 424, p. 810.
4. Bockelmann, U., *Curr. Opin. Struct. Biol.*, 2004, vol. 14, p. 368.
5. Sasaki, K., Koshioka, M., Misawa, H., et al., *Opt. Lett.*, 1991, vol. 16, p. 1463.
6. Liesener, J., Reicherter, M., Haist, T., and Tiziani, H.J., *Opt. Commun.*, 2000, vol. 185, p. 77.
7. Doering, W.E. and Nie, S.M., *Anal. Chem.*, 2003, vol. 75, p. 6171.
8. Gao, X.H. and Nie, S.M., *Anal. Chem.*, 2004, vol. 76, p. 2406.
9. Behrend, C.J., Anker, J.N., and Kopelman, R., *Appl. Phys. Lett.*, 2004, vol. 84, p. 154.
10. Behrend, C.J., Anker, J.N., McNaughton, B.H., et al., *J. Phys. Chem.*, 2004, vol. 108, p. 10408.
11. Agayan, R.R., Gittes, F., Kopelman, R., and Schmidt, C.F., *Appl. Opt.*, 2002, vol. 41, p. 2318.
12. Harada, Y. and Asakura, T., *Opt. Commun.*, 1996, vol. 124, p. 529.
13. Gordon, J.P., *Phys. Rev. A*, 1973, vol. 8, p. 14.
14. Ashkin, A., Dziedzic, J.M., Bjorkholm, J.E., and Chu, S., *Opt. Lett.*, 1986, vol. 11, p. 288.
15. Agayan, R.R., Horvath, T., McNaughton, H., et al., *Proc. SPIE*, 2004, vol. 5514, p. 502.
16. Siiman, O., Jitianu, A., Bele, M., et al., *J. Colloid Interface Sci.*, 2007, vol. 309, p. 8.
17. Zhao, G.-F., Zhi, L.-L., and Guo, L.-J., *J. Chem. Phys.,* 2007, vol. 127, p. 234705.
18. Tangney, P. and Scandolo, S., *J. Chem. Phys.,* 2002, vol. 117, p. 8898.
19. Girifalco, L.A. and Weizer, V.G., *Phys. Rev.*, 1959, vol. 114, p. 687.
20. Sato, S., Chen, D.-R., and Pui, D.Y.H., *Aerosol Air Quality Res.*, 2007, vol. 7, p. 278.
21. Lemberg, H.L. and Stillinger, F.H., *J. Chem. Phys.*, 1975, vol. 62, p. 1677.
22. Rahman, A., Stillinger, F.H., and Lemberg, H.L., *J. Chem. Phys.*, 1975, vol. 63, p. 5223.
23. Saint-Martin, H., Hess, B., and Berendsen, H.J.C., *J. Chem. Phys.*, 2004, vol. 120, p. 11133.
24. Le Bail, A., *J. Appl. Crystallogr.*, 2005, vol. 38, p. 389.
25. Haile, J.M., *Molecular Dynamics Simulation. Elementary Methods*, New York: Wiley, 1992.
26. Koshlyakov, V.N., *Zadachi dinamiki tverdogo tela i prikladnoi teorii giroskopov* (Problems of Solid Body Dynamics and Applied Theory of Gyroscopes), Moscow: Nauka, 1985.
27. Sonnenschein, R., *J. Comput. Phys.*, 1985, vol. 59, p. 347.
28. Galashev, A.E., *Russ. J. Phys. Chem. A*, 2009, vol. 83, p. 2249.
29. Neumann, M., *J. Chem. Phys.*, 1985, vol. 82, p. 5663.
30. Bosma, W.B., Fried, L.E., and Mukamel, S., *J. Chem. Phys.*, 1993, vol. 98, p. 4413.
31. *Fizicheskaya entsiklopediya* (Physical Encyclopedia), Prokhorov, A.M., Ed., Moscow: Sovetskaya Entsiklopediya, 1988, vol. 1.
32. Landau, L., Lifshitz, E., and Pitaevski, L., *Electrodynamics of Continuous Media*, Oxford: Pergamon, 1984.
33. Duran, A., Serna, C., Fornes, V., and Fernandez, Navarro, J.M., *J. Non-Cryst. Solids*, 1986, vol. 82, p. 69.
34. Ocana, M., Fornes, V., Garcia-Ramos, J.V., and Serna, C.J., *Phys. Chem. Miner.*, 1987, vol. 14, p. 527.
35. Izaak, T.I., Babkina, O.V., Lapin, I.N., et al., *Nanotekhnika*, 2006, no. 4, p. 34.
36. Kingma, K.J. and Hemley, R.J., *Am. Mineral.*, 1994, vol. 79, p. 269.
37. Bruckner, R., *J. Non-Cryst. Solids*, p. 1970.
38. Novruzova, O.A., Rakhmanova, O.R., and Galashev, A.E., *Zh. Fiz. Khim.*, 2007, vol. 81, p. 1825.